

## **Bacteria-photocatalyst sheet for sustainable carbon capture and utilisation**

Qian WANG,<sup>1,†</sup> Shafeer KALATHIL,<sup>1,2,†</sup> Chanon PORNRUNGROJ,<sup>1</sup> Constantin D. SAHM,<sup>1</sup> Erwin REISNER<sup>1,\*</sup>

### **Affiliation and full postal address**

1 *Yusuf Hamied Department of Chemistry, University of Cambridge, Lensfield Road, Cambridge CB2 1EW, UK*

2 *Hub for Biotechnology in the Built Environment, Department of Applied Sciences, Faculty of Health and Life Sciences, Northumbria University, Newcastle upon Tyne, NE1 8ST, UK*

† Equal contribution

### **\*Corresponding author**

Professor Erwin REISNER

*Yusuf Hamied Department of Chemistry, University of Cambridge, Lensfield Road, Cambridge CB2 1EW, UK*

Tel: +44-1223336323

E-mail: [reisner@ch.cam.ac.uk](mailto:reisner@ch.cam.ac.uk)

## Abstract

The clean conversion of carbon dioxide and water to a single multicarbon product and O<sub>2</sub> using sunlight via photocatalysis without the assistance of organic additives or electricity remains an unresolved challenge. Here we report a bio-abiotic hybrid system with the nonphotosynthetic, CO<sub>2</sub>-fixing acetogenic bacterium, *Sporomusa ovata* (*S. ovata*) grown on a scalable and cost-effective photocatalyst sheet consisting of a pair of particulate semiconductors (La and Rh co-doped SrTiO<sub>3</sub> (SrTiO<sub>3</sub>:La,Rh) and Mo-doped BiVO<sub>4</sub> (BiVO<sub>4</sub>:Mo)). The biohybrid effectively produces acetate (CH<sub>3</sub>COO<sup>-</sup>) and oxygen (O<sub>2</sub>) using only sunlight, CO<sub>2</sub> and H<sub>2</sub>O, achieving a solar-to-acetate conversion efficiency of 0.7%. The photocatalyst sheet oxidises water to O<sub>2</sub> and provides electrons and hydrogen (H<sub>2</sub>) to *S. ovata* for the selective synthesis of CH<sub>3</sub>COO<sup>-</sup> from CO<sub>2</sub>. To demonstrate the utility in a closed carbon cycle, the solar-generated acetate was used directly as feedstock in a bioelectrochemical system for electricity generation. These semi-biological systems thus offer a promising strategy for sustainably and cleanly fixing CO<sub>2</sub> and closing the carbon cycle.

Artificial photosynthesis aims to convert H<sub>2</sub>O and CO<sub>2</sub> with intermittent solar energy into storable fuels. The sunlight-driven CO<sub>2</sub> reduction reaction (CO<sub>2</sub>RR) to form multicarbon products (C<sub>2/2+</sub>) using inorganic catalysts is challenging because they typically provide poor selectivity toward C<sub>2/2+</sub> products and necessitate additional electricity input to offset the large overpotential requirements.<sup>1-6</sup> In contrast, nonphotosynthetic, CO<sub>2</sub>-fixing bacteria have metabolic pathways that can produce C<sub>2/2+</sub> from CO<sub>2</sub> with high selectivity and display relatively high stability toward environmental perturbations.<sup>7-11</sup> Thus, hybrid bio-abiotic systems consisting of synthetic light absorbers assembled with CO<sub>2</sub>-fixing bacteria provide the opportunity for solar-powered CO<sub>2</sub>-to-C<sub>2/2+</sub> conversion, which harnesses the efficient light-harvesting capabilities of semiconductors and the strong catalytic power of living biocatalysts.<sup>9,12</sup>

Among several prototypes of such hybrid bio-abiotic systems for photosynthetic CO<sub>2</sub> fixation, photovoltaic-driven electrolysis or photoelectrochemical (PEC) cells are under development.<sup>13-17</sup> These approaches either rely on large quantities of an intermediate fuel such as H<sub>2</sub> or syngas being generated to feed the bacteria in a separate compartment or suffer from local pH gradients and IR drops (a potential drop due to solution resistance) occurring during the redox reactions in a close to neutral pH solution when directly integrated into (photo)electrodes.<sup>18,19</sup> Additionally, the preparation of solar cells and (photo)electrodes is typically complex, often requiring vacuum processes.<sup>14,15,20-22</sup>

A more straightforward route to establish bio-abiotic hybrids is to apply a colloidal system that uses particulate photocatalysts attributable to their simpler design and potentially lower cost.<sup>22-24</sup> However, colloidal biohybrid systems require commonly the addition of sacrificial reagents,<sup>25-27</sup> as the photosensitiser is usually unable to catalyse water oxidation. Cysteine has been widely used as a sacrificial electron donor to quench the photogenerated holes, exemplified by the CO<sub>2</sub>-to-acetate reducing photobiohybrid of *Moorella thermoacetica*|CdS (*M. thermoacetica*|CdS).<sup>26</sup> However, a recent study showed acetate production in this biohybrid system even in the absence of light and

demonstrated a cysteine-dependent metabolic pathway for acetate production.<sup>28</sup> Cysteine is also a known electron mediator for microbial respiration,<sup>29,30</sup> and functioned as an electron donor in iron reduction by *Shewanella* species.<sup>30</sup> Thus, sacrificial reagents and organic additives should be avoided in the development of photobiohybrid systems to achieve sustainable and clean CO<sub>2</sub> conversion.

Constructing Z-scheme systems using two complementary light harvesters for photoreduction and photooxidation, respectively, provides a platform to drive CO<sub>2</sub>RR and water oxidation simultaneously without sacrificial reagents or organic mediators.<sup>31</sup> However, Z-scheme systems using bio-abiotic hybrids remain scarce because of the difficulty to establish efficient interparticle electron transfer between the light absorbers. An attempt has been made to combine *M. thermoacetica*|CdS with a TiO<sub>2</sub> nanoparticle loaded with a manganese(II) phthalocyanine, using a cysteine/cystine redox couple as the electron relay.<sup>17</sup> This tandem system has been reported to produce acetate and O<sub>2</sub> simultaneously, but the efficiency and stability are limited due to side reactions caused by the redox couple.

Monolithic photocatalyst sheets contain an immobilised pair of semiconductor nanoparticles with narrow bandgaps (e.g. SrTiO<sub>3</sub>:La,Rh and BiVO<sub>4</sub>:Mo) on a conductive inorganic layer (e.g. gold and carbon).<sup>19,32</sup> These photocatalyst sheets can achieve unassisted, scalable, and efficient light-driven water splitting and CO<sub>2</sub>-to-formate conversion as the interparticle electron transfer is facilitated by solid conductive mediators. Furthermore, the reduction and oxidation reactions occur in close vicinity in the photocatalyst sheets, which can largely suppress the local pH changes during the redox reactions.<sup>32</sup> The photocatalyst sheets display pH-independent (pH 2.5-7.5) activity and therefore achieve overall water splitting without adjusting the pH or adding buffer.<sup>33</sup> The photocatalyst sheet design is thus expected to overcome the hurdles commonly observed in (photo)electrochemical and conventional photocatalytic colloidal systems and is a particularly

promising platform for the assembly of hybrid bio-abiotic systems due to the high solar-to-fuel conversion efficiency operating at a biocompatible neutral pH.

Here we report that a photocatalyst sheet ( $\text{Cr}_2\text{O}_3/\text{Ru-SrTiO}_3:\text{La,Rh}|\text{ITO}|\text{RuO}_2\text{-BiVO}_4:\text{Mo}$ ), which is prepared by a relatively inexpensive and readily accessible drop-casting method, combined with  $\text{CO}_2$ -fixing acetogenic bacteria (*S. ovata*) results in selective  $\text{CH}_3\text{COO}^-$  production coupled to  $\text{O}_2$  evolution using only sunlight,  $\text{CO}_2$ , and  $\text{H}_2\text{O}$ , with a solar-to-acetate conversion efficiency (STA) of  $0.70 \pm 0.04\%$ . The electrons and protons for the  $\text{CO}_2\text{RR}$  must be sourced from  $\text{H}_2\text{O}$  without the consumption of sacrificial reagents in order to develop a sustainable process. However, reports of photocatalytic  $\text{CO}_2\text{RR}$  conjugated to water oxidation remain scarce.<sup>34</sup> This system does not require the addition of organics as a sacrificial reagent or redox couples, thereby demonstrating clean  $\text{CO}_2$ -to-multicarbon conversion using hybrid biocatalysis at benchmark efficiency.

## Results

### Assembly of the biohybrid system

*S. ovata* was selected as a microbe because it can efficiently catalyse the  $\text{CO}_2\text{RR}$  to  $\text{CH}_3\text{COO}^-$  by using  $\text{H}_2$  or electrons directly from an electrode in microbial electrosynthesis.<sup>14,35</sup>  $\text{SrTiO}_3:\text{La,Rh}$  and  $\text{BiVO}_4:\text{Mo}$  nanoparticles were chosen as light harvesters in the Z-scheme photocatalysts (Figure 1a and Supplementary Fig.1), because they can absorb visible light, with an absorption edge of 520 nm (Supplementary Fig.2).<sup>19,36</sup> Indium tin oxide (ITO) nanoparticles (Supplementary Fig.1) act as charge mediators to connect  $\text{SrTiO}_3:\text{La,Rh}$  and  $\text{BiVO}_4:\text{Mo}$  particles and display high transparency to visible light without catalysing side-reactions (i.e.  $\text{O}_2$  reduction reaction).<sup>37,38</sup>

The  $\text{SrTiO}_3:\text{La,Rh}|\text{ITO}|\text{BiVO}_4:\text{Mo}$  sheet (Figure 1b and Supplementary Fig. 3 and 4) was prepared by readily accessible and scalable drop-casting (see Methods). The  $\text{Cr}_2\text{O}_3/\text{Ru}$  and  $\text{RuO}_2$  were subsequently loaded on the  $\text{SrTiO}_3:\text{La,Rh}$  and  $\text{BiVO}_4:\text{Mo}$  by photodeposition, respectively, to

construct the H<sub>2</sub> evolution photocatalyst (Cr<sub>2</sub>O<sub>3</sub>/Ru-SrTiO<sub>3</sub>:La,Rh) and the O<sub>2</sub> evolution photocatalyst (RuO<sub>2</sub>-BiVO<sub>4</sub>:Mo) (Figure 1a). The Ru and RuO<sub>2</sub> nanoparticles provide active sites for H<sub>2</sub> and O<sub>2</sub> evolution, respectively, whereas the Cr<sub>2</sub>O<sub>3</sub> shell prevents access of O<sub>2</sub> molecules to the Ru surface and thereby suppresses the occurrence of the competitive O<sub>2</sub> reduction reaction.<sup>19,39</sup> The loading amounts of Ru and Cr were estimated via inductively coupled plasma–optical emission spectrometry (ICP–OES) to be ~68 and ~20 nmol cm<sup>-2</sup> (geometrical surface area of sheet), respectively (Supplementary Table 1).

Scanning electron microscopy and energy dispersive X-ray spectroscopy (SEM–EDX) mapping images of the photocatalyst sheet (Supplementary Fig. 3 and 4) revealed the formation of a particle layer containing the SrTiO<sub>3</sub>:La,Rh, BiVO<sub>4</sub>:Mo, and ITO with a thickness of ~10 μm. The ITO nanoparticles aggregated to form large clusters, connecting the SrTiO<sub>3</sub>:La,Rh and BiVO<sub>4</sub>:Mo and providing pathways for interparticle electron transfer.<sup>37,38</sup> The stacked particle layer with interparticle voids (several micrometres in diameter) is expected to provide easy access for bacterial colonization.<sup>40</sup>

The *S. ovata*|sheet hybrid was assembled by immersing the Cr<sub>2</sub>O<sub>3</sub>/Ru-SrTiO<sub>3</sub>:La,Rh|ITO|RuO<sub>2</sub>-BiVO<sub>4</sub>:Mo sheet (Supplementary Fig. 5 and 6) in an *S. ovata* medium (Supplementary Table 2). The sheet split water into H<sub>2</sub> and O<sub>2</sub> under light irradiation and acted as the sole electron and/or H<sub>2</sub> donor for the bacteria metabolism, leading to the growth of *S. ovata* onto the sheet during the photosynthetic reaction.

### **Photosynthetic activity**

The water-splitting ability of the Cr<sub>2</sub>O<sub>3</sub>/Ru-SrTiO<sub>3</sub>:La,Rh|ITO|RuO<sub>2</sub>-BiVO<sub>4</sub>:Mo sheet (~2.2 cm<sup>2</sup>) in the *S. ovata* medium (without the bacterium) purged with N<sub>2</sub> (pH 6.9) was confirmed under simulated solar irradiation (Air Mass 1.5 Global (AM 1.5G) filter, 100 mW cm<sup>-2</sup>). The sheet split

water into H<sub>2</sub> and O<sub>2</sub> in a stoichiometric ratio with a solar-to-hydrogen conversion efficiency of 0.62 ± 0.04% without forming any CO<sub>2</sub>RR products (Supplementary Fig. 7 and Supplementary Table 3 and 4).

The CO<sub>2</sub>RR was subsequently performed by using the same reaction medium purged with 80%N<sub>2</sub>/20%CO<sub>2</sub> (pH 7.0) containing *S. ovata* cells (final optical density at 600 nm: 0.6). The biohybrid system produced CH<sub>3</sub>COO<sup>-</sup> (~ 9 mM) and O<sub>2</sub> simultaneously in the expected 1:2 ratio (Figure 2a) under 1 sun illumination, demonstrating closed redox cycle catalysis and ruling out that the presence of impurities functioned as sacrificial reductant/oxidant. Proton nuclear magnetic resonance (<sup>1</sup>H NMR) spectroscopy (Supplementary Fig. 8) and gas chromatography confirmed that CH<sub>3</sub>COO<sup>-</sup> is the only detectable product of CO<sub>2</sub>RR, with a small amount of H<sub>2</sub> also being detected (4.6 ± 0.9 μmol cm<sup>-2</sup> in 15 h). Accordingly, the selectivity for CH<sub>3</sub>COO<sup>-</sup> formation in the reduction reactions is ~90 % (~100% in CO<sub>2</sub>RR). The photograph and SEM-EDX mapping images of the sample after the reaction (Figure 1c and 3 and Supplementary Fig. 1) revealed the presence of all components, including the *S. ovata* cells, on the photocatalyst sheet. Additionally, the concentrations of protein in the medium before the reaction and on the sheet (~2.2 cm<sup>2</sup>) after the reaction were estimated as 1.55 ± 0.18 and 0.59 ± 0.03 mg, respectively, further supporting that part of the *S. ovata* cells grow on the photocatalyst sheet surface during the photosynthetic reaction.

The formation of CH<sub>3</sub>COO<sup>-</sup> was observed for λ ≤ 510 nm irradiation (Figure 2c), consistent with the absorption onsets of both SrTiO<sub>3</sub>:La,Rh and BiVO<sub>4</sub>:Mo. An STA of 0.70 ± 0.04% was obtained and the apparent quantum yield (AQY) was 21.3% at 420 ± 15 nm. The AQY decreased with increasing wavelength of incident photons up to 510 nm, which is in reasonably good agreement with the diffuse reflectance spectra observed for SrTiO<sub>3</sub>:La,Rh and BiVO<sub>4</sub>:Mo. These results support an efficient Z-scheme mechanism derived by the photoexcited electron-hole pairs in the SrTiO<sub>3</sub>:La,Rh and BiVO<sub>4</sub>:Mo. The STA is higher than that of a tandem PEC cell composed of silicon nanowires as

the photocathode and titanium dioxide nanowires as the photoanode (0.38%).<sup>14</sup> The pH gradient and IR drop during the redox reaction on the photocatalyst sheet are also largely suppressed and the presented system does therefore not require a strong electrolyte and buffer as required in classical PEC cells.<sup>32</sup> In comparison to PEC cells, the preparation of photocatalyst sheet-bacteria hybrid is also less complicated and does not require vacuum processes, making it a relatively cost-effective process and provides the basis to scale-up the photosynthetic activity.

Isotopic labelling experiments showed that  $^{13}\text{CO}_2/\text{H}^{13}\text{CO}_3^-$  was the sole carbon source for  $\text{CH}_3\text{COO}^-$  production (Figure 2d and Supplementary Fig. 9).  $^1\text{H}$  NMR spectroscopy (Figure 2d) exhibited a doublet attributable to the  $^{13}\text{C}$ -coupled proton with  $^1J_{\text{CH}} = 127$  Hz and  $^2J_{\text{CH}} = 6$  Hz, which is consistent with previous reports<sup>41</sup> and the spectrum for an authentic sample of  $^{13}\text{CH}_3^{13}\text{COONa}$  (Supplementary Fig. 10). The amount of  $^{13}\text{CH}_3^{13}\text{COO}^-$  was decreased by half compared to  $^{12}\text{CO}_2/\text{H}^{12}\text{CO}_3^-$  conditions (Supplementary Table 4), a phenomenon previously assigned to the propagation of isotopes through metabolic networks and their affected operation by kinetic isotope effects.<sup>42,43</sup>

No products were detected in a series of deletional control experiments in which light,  $\text{SrTiO}_3:\text{La,Rh}$ , and  $\text{BiVO}_4:\text{Mo}$  were systematically removed (Supplementary Table 4). The experiments without *S. ovata*. or using heat-killed *S. ovata* cells did not yield any  $\text{CO}_2\text{RR}$  products (Supplementary Tables 3 and 4), thereby confirming that live bacteria are required for the  $\text{CO}_2\text{RR}$ .

A system employing the photocatalyst sheet in a separate compartment from *S. ovata* with the headspace connecting the two chambers (accumulated  $\text{H}_2$  concentration of ~6% after 15 h irradiation) produced only ~16% acetate of that obtained from the *S. ovata*|sheet hybrids (Figure 2b). The  $\text{O}_2$  evolved accompanied the reduction reactions in a stoichiometric ratio of  $(\text{CH}_3\text{COO}^- + \text{H}_2): \text{O}_2 = 2.1 \pm 0.1$ . However, the selectivity of acetate in the obtained products from reduction reactions is only ~7%. This result suggests that growing the bacteria directly at the  $\text{H}_2$  evolution site (Figure 3) enables



the biocatalyst to operate under high local H<sub>2</sub> concentrations, avoiding the need for the accumulation of high concentrations of bulk H<sub>2</sub> in the headspace.<sup>44</sup>

### CO<sub>2</sub>-to-CH<sub>3</sub>COO<sup>-</sup> conversion pathways

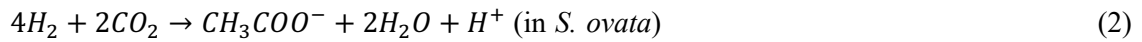
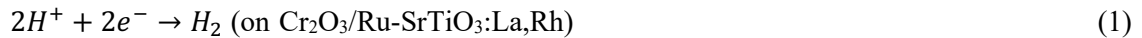
A bacteria-photocatalyst sheet in the absence of the proton reduction cocatalyst Cr<sub>2</sub>O<sub>3</sub>/Ru on the SrTiO<sub>3</sub>:La,Rh surface (Supplementary Table 3) was studied for the artificial photosynthesis reaction. This system also produced CH<sub>3</sub>COO<sup>-</sup> from CO<sub>2</sub> and H<sub>2</sub>O (O<sub>2</sub>:CH<sub>3</sub>COO<sup>-</sup> = 1.9±0.1) under the same reaction conditions, but the product amounts in 15 h were approximately 80% lower than those observed from the hybrids with Cr<sub>2</sub>O<sub>3</sub>/Ru loading. The direct utilisation of electrons is consistent with a previous report, where a graphite electrode acted as the electron donor for *S. ovata* to convert CO<sub>2</sub> into CH<sub>3</sub>COO<sup>-</sup>.<sup>35</sup> Thus, *S. ovata* can use both H<sub>2</sub> and electrons delivered directly to the cells with the photocatalyst sheet for CH<sub>3</sub>COO<sup>-</sup> formation from CO<sub>2</sub> (Figure 1a).

No CH<sub>3</sub>COO<sup>-</sup> was detected in a colloidal system after 15 h irradiation (1 sun), where RuO<sub>2</sub>-BiVO<sub>4</sub>:Mo powders and *S. ovata* were suspended in the reaction medium. This observation suggests that RuO<sub>2</sub>-BiVO<sub>4</sub>:Mo could not directly provide *S. ovata* with electrons, possibly due to insufficient driving force from its conduction band (Figure 1a).

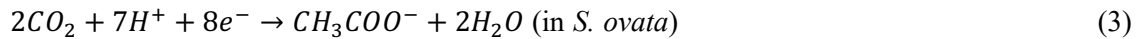
Accordingly, we conclude that CH<sub>3</sub>COO<sup>-</sup> and O<sub>2</sub> are produced by the following mechanism: photoexcitation produces electrons and holes in both SrTiO<sub>3</sub>:La,Rh and BiVO<sub>4</sub>:Mo when the photocatalyst sheet is exposed to simulated sunlight. The visible light absorption ability of SrTiO<sub>3</sub>:La,Rh is due to photoexcitation from the donor levels formed by Rh<sup>3+</sup> ions to its conduction band.<sup>36</sup> In addition, the photoexcited electrons transfer smoothly from BiVO<sub>4</sub>:Mo to SrTiO<sub>3</sub>:Rh via the ITO nanoparticles.<sup>38</sup> Therefore, the photoexcited electrons in BiVO<sub>4</sub>:Mo transferred to SrTiO<sub>3</sub>:La,Rh and recombined with the holes on the donor levels formed by Rh<sup>3+</sup> to achieve the Z-scheme photocatalytic reaction. The SrTiO<sub>3</sub>:La,Rh is unable to achieve overall water splitting to

produce both H<sub>2</sub> and O<sub>2</sub> (ref. <sup>33</sup>) and the BiVO<sub>4</sub>:Mo cannot generate H<sub>2</sub> via proton reduction because its conduction band minimum is more positive than the H<sup>+</sup> to H<sub>2</sub> reduction potential,<sup>45</sup> and the H<sub>2</sub> and O<sub>2</sub> production reactions therefore take place on Cr<sub>2</sub>O<sub>3</sub>/Ru-SrTiO<sub>3</sub>:La,Rh and RuO<sub>2</sub>-BiVO<sub>4</sub>:Mo, respectively, accomplishing via the overall water-splitting reaction. The produced H<sub>2</sub> is taken by *S. ovata* to perform CO<sub>2</sub>RR and produces CH<sub>3</sub>COO<sup>-</sup> via the acetyl-CoA Wood-Ljungdahl pathway (Figure 1a). Additionally, *S. ovata* can use photogenerated electrons from illuminated SrTiO<sub>3</sub>:La,Rh nanoparticles to perform photosynthesis. The overall photosynthetic pathways are:

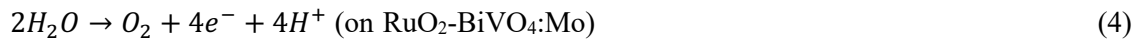
Cathodic reaction:



Or



Anodic reaction:



Overall reaction:



The production of H<sub>2</sub> with Cr<sub>2</sub>O<sub>3</sub>/Ru-SrTiO<sub>3</sub>:La,Rh powder suspended in an aqueous solution containing 18 mM CH<sub>3</sub>COO<sup>-</sup> after 15 h irradiation (pH 8.1; 1 sun) was negligible (< 2 μmol cm<sup>-2</sup>) and the amount of CH<sub>3</sub>COO<sup>-</sup> did not change substantially. Moreover, similar photocurrents for the RuO<sub>2</sub>-BiVO<sub>4</sub>:Mo|Au photoanode were observed with and without the presence of 18 mM CH<sub>3</sub>COO<sup>-</sup> (Supplementary Fig. 11). Therefore, CH<sub>3</sub>COO<sup>-</sup> was not oxidised by the holes in either SrTiO<sub>3</sub>:La,Rh or BiVO<sub>4</sub>:Mo in significant amounts, supporting that it does not serve as an electron scavenger in the hybrid system. These observations highlight the clean CO<sub>2</sub>-to-CH<sub>3</sub>COO<sup>-</sup> conversion in the current system without substantial limitations from the back reaction with accumulated acetate.

### System stability and viability

The  $\text{CH}_3\text{COO}^-$  and  $\text{O}_2$  generation rates decreased slowly during the 15 h reaction (Figure 2a). The biological toxicity of each component in the photocatalyst sheet ( $\text{Cr}_2\text{O}_3/\text{Ru-SrTiO}_3:\text{La,Rh}$ , ITO,  $\text{RuO}_2\text{-BiVO}_4:\text{Mo}$ ) was determined by growing bacteria in presence of individual component powders (Supplementary Fig. 12) and showed that the production of acetate did not change significantly when the bacteria were grown in the presence of  $\text{Cr}_2\text{O}_3/\text{Ru-SrTiO}_3:\text{La,Rh}$ , ITO or  $\text{RuO}_2\text{-BiVO}_4:\text{Mo}$ , indicating that these components are not toxic to *S. ovata*. As the gas evolution rates over the bacteria-free  $\text{Cr}_2\text{O}_3/\text{Ru-SrTiO}_3:\text{La,Rh}|\text{ITO}|\text{RuO}_2\text{-BiVO}_4:\text{Mo}$  sheet also decreased during water splitting (Supplementary Fig. 7), the drop in activity of the hybrid was assigned to the deactivation of the photocatalyst sheet. The sheet exhibited similar diffuse-reflectance spectra before and after the photosynthetic reaction (Supplementary Fig. 2), indicating an unchanged light absorption of the semiconductors upon the loading of microbes. No notable differences in the phases of  $\text{SrTiO}_3:\text{La,Rh}$ ,  $\text{BiVO}_4:\text{Mo}$ , and ITO were observed in the X-ray diffraction patterns of the sheet before and after a 15 h water-splitting reaction (Supplementary Fig. 13). The ICP-OES analysis suggested that the Ru amount did not notably change after the water-splitting reaction, but the amount of Cr decreased by ~30% (Supplementary Table 1), demonstrating the partial dissolution of  $\text{Cr}_2\text{O}_3$ .<sup>37</sup>

The  $\text{Cr}_2\text{O}_3$  was then reloaded on the photocatalyst sheet after a 15 h irradiation. The reaction was restarted by inserting the sheet with reloaded  $\text{Cr}_2\text{O}_3$  and adding the recycled bacteria into a fresh reactant medium purged with 80% $\text{N}_2$ /20% $\text{CO}_2$  (see Methods). The photosynthetic reaction was carried out for 3 runs of 15 h (Figure 4a). The amounts of formed  $\text{CH}_3\text{COO}^-$  and  $\text{O}_2$  in the third run were 82% of the initial run even using the recycled bacteria by centrifuging, confirming that bacteria were active within 45 h operation and demonstrating the reusability of the bacterial catalysts. The pH of the reaction medium remained stable (pH 7.2) after each 15-hour photosynthetic reaction. No

obvious changes on the morphologies of photocatalyst sheet were observed after the 45-h reaction, except for the bacteria loading (Supplementary Fig. 14 and 15). The stability for the continuous operation without reloading the Cr<sub>2</sub>O<sub>3</sub> could be enhanced by photodepositing TiO<sub>2</sub>/CoOOH on the photocatalyst surface to suppress the dissolution of Cr<sub>2</sub>O<sub>3</sub> in the cocatalyst.<sup>46</sup>

A high O<sub>2</sub> concentration (> 10%) in the reactor was found to be harmful to *S. ovata*, resulting in in stoichiometric acetate and O<sub>2</sub> production by the *S. ovata*|sheet hybrid. Control experiments show that the CH<sub>3</sub>COO<sup>-</sup> production activity and therefore *S. ovata* growth was not affected by the presence of 4% headspace O<sub>2</sub> (Supplementary Fig. 16). The reactor cell was therefore designed and optimized to ensure that the O<sub>2</sub> concentration did not exceed 4%. The O<sub>2</sub> concentration accumulated in the reactor headspace of the *S. ovata*|sheet hybrid system after 15 h is 3-4%, which is sufficiently low for the bacterium to operate. Activity of strict anaerobes in the presence of O<sub>2</sub> is not unprecedented,<sup>47</sup> because the presence of enzymes such as superoxide reductase,<sup>48</sup> superoxide dismutase,<sup>49</sup> rubredoxins<sup>50</sup> and NADH<sup>51</sup> oxidase enable protection from O<sub>2</sub> damage. For example, *Geobacter sulfurreducens* (*G. sulfurreducens*), which was previously classified as a strict anaerobe, can survive at low O<sub>2</sub> concentration due to the expression of these oxidative stress enzymes (superoxide dismutase, superoxide reductase, rubredoxins, A-type flavodoxins).<sup>52</sup> *Desulfovibrio* species can also grow when exposed to O<sub>2</sub> by expressing oxidative stress enzymes,<sup>53</sup> and anaerobic homoacetogenic bacteria isolated from terminate guts can reduce O<sub>2</sub> to provide favourable conditions for their growth.<sup>54</sup> The genome of *S. ovata* also shows the presence of superoxide dismutase, rubredoxins and flavodoxins, which suggests the ability of surviving at least under low O<sub>2</sub> concentrations.<sup>55</sup> The pH of the reaction medium did not change considerably after 15 h photosynthetic reaction (pH 7.2).

As CO<sub>2</sub> with concentrations of 5-20% is available from coal-fired power plants and many industrial processes,<sup>56</sup> CO<sub>2</sub> concentration in the purged gas was adjusted from 5 to 20% to investigate its effect on the photosynthetic activity of the *S. ovata*|sheet hybrid system (Figure 4b). The product

generation rates and the selectivity of  $\text{CH}_3\text{COO}^-$  did not dramatically change over this  $\text{CO}_2$  concentration range, suggesting that the hybrid system can effectively produce  $\text{CH}_3\text{COO}^-$  from  $\text{CO}_2$  with relatively low concentrations.

### **Power generation from solar-produced acetate**

Acetate can be used as a raw material for producing numerous chemicals, including polyvinyl acetate, cellulose acetate, metal acetates, vinyl acetate monomer, volatile organic esters, and alkanes used in making food-grade vinegar, plastics, photographic products, paints, and pharmaceuticals.<sup>57</sup> Additionally, it can be used as fuel in microbial fuel cells that integrate electroactive bacteria into electrodes for chemical-to-electricity conversion upon demand.<sup>40,58,59</sup>

To demonstrate accumulation of meaningful quantities and in situ utilisation of acetate from our biohybrid system, we directly used the reaction medium obtained from the 15 h artificial photosynthetic reaction over the *S. ovata*|sheet (contained  $\sim 9$  mM  $\text{CH}_3\text{COO}^-$ ; without removing *S. ovata* cells) as feedstock for a bioelectrochemical anode of a microbial fuel cell (Figure 5a). The bioelectrochemical system consisted of a previously reported porous inverse opal-ITO electrode (IO-ITO, porosity:  $\sim 10$   $\mu\text{m}$ )<sup>40</sup> inoculated with *G. sulfurreducens* (Supplementary Fig. 17). *G. sulfurreducens* is an electric bacterium that can grow using  $\text{CH}_3\text{COO}^-$  as the electron donor and uses the electrode as the electron acceptor.<sup>58,59</sup> A control experiment in the absence of acetate demonstrates that *G. sulfurreducens* is incapable of generating current (Supplementary Fig. 18). At a potential of 0.1 V vs. standard hydrogen electrode (SHE), *G. sulfurreducens* started to produce current by metabolizing  $\text{CH}_3\text{COO}^-$  into  $\text{CO}_2$  with a maximum current density of  $3.08 \pm 0.12$   $\text{mA cm}^{-2}$  and a Faradaic efficiency of  $88.2 \pm 6.6\%$  for  $\text{CH}_3\text{COO}^-$  oxidation, which is comparable with the reported benchmark performance ( $3$   $\text{mA cm}^{-2}$ ) for microbial electrogenesis.<sup>40</sup> Thus, the  $\text{CH}_3\text{COO}^-$  generated by the *S. ovata*|sheet hybrids can directly serve as a fuel in a microbial fuel cell to produce electricity

upon demand without the removal of *S. ovata* and the extraction and purification of yielded acetate. This demonstration serves as an illustration for a closed carbon cycle, where solar energy is stored by converting CO<sub>2</sub> into acetate and released back to CO<sub>2</sub> when producing renewable electricity.

## Conclusions

We have established a strategy to combine the high selectivity of a biological catalyst for clean CO<sub>2</sub>-to-C<sub>2</sub> conversion with the light-harvesting and water-splitting ability of semiconductors without the need for organic additives or external bias voltage. The efficient bio-abiotic hybrid prototype (*S. ovata*|Cr<sub>2</sub>O<sub>3</sub>/Ru-SrTiO<sub>3</sub>:La,Rh|ITO|RuO<sub>2</sub>-BiVO<sub>4</sub>:Mo photocatalyst sheet) produced multi-carbon liquid fuel (CH<sub>3</sub>COO<sup>-</sup>) and O<sub>2</sub> in a 1:2 stoichiometric ratio from CO<sub>2</sub> and H<sub>2</sub>O using sunlight as the sole energy input, achieving an STA of 0.70 ± 0.04%. The efficient CO<sub>2</sub> fixation over 45 hours and stability benefited from the high viability of *S. ovata*. Additionally, the obtained CH<sub>3</sub>COO<sup>-</sup> can be fed into a biohybrid fuel cell to generate electricity and thereby closes the carbon cycle. The presented bio-abiotic system is comprised of scalable components (photocatalyst sheet and bacteria) and the materials and device preparation is readily accessible and relatively cost-effective without the requirement for vacuum processes. The hybrids operated under ambient conditions (298 K, 1 atm) with relatively low CO<sub>2</sub> concentrations (5-20%), thereby representing a promising strategy towards a practical application of artificial photosynthesis.

The water splitting activity of the present Cr<sub>2</sub>O<sub>3</sub>/Ru-SrTiO<sub>3</sub>:La,Rh|ITO|RuO<sub>2</sub>-BiVO<sub>4</sub>:Mo photocatalyst sheet is limited by the short absorption edge wavelengths of SrTiO<sub>3</sub>:La,Rh and BiVO<sub>4</sub>:Mo (~520 nm). The efficiency can be improved by replacing the photocatalyst with narrower bandgap energies. Additionally, genetic engineering would allow for the modification of the electron uptake pathway in acetogenic bacteria in order to increase CO<sub>2</sub> conversion while also redirecting the electron flux to medium-chain fatty acids (e.g., butyric acid) and other higher value products instead

of the natural product acetate.<sup>7,60</sup> Furthermore, designing a flow reactor can avoid product inhibition to bacteria which can lead to better performance. For example, the current design is compatible with large area photocatalyst sheet reactors (up to 100 m<sup>2</sup>),<sup>61</sup> where products can be readily extracted from the reaction chamber. The assembly of bacteria on the sheet is straightforward and allows for a large degree of versatility by combining various bacteria and semiconductors to produce a diverse range of solar fuels and chemicals in the future.

## **Methods**

### **Culturing of *S. ovata***

The strain *S. ovata* was purchased from DSMZ-German Collection of Microorganisms and Cell Cultures GmbH (DSM No.: 2662). *S. ovata* cells were grown using betaine as the electron donor in the DSMZ-recommended growth medium (DSMZ 311) with casitone, Na-resazurin solution, and Na<sub>2</sub>S were omitted (Supplementary Table 2). The medium was purged with a mixture of 20%CO<sub>2</sub> and 80%N<sub>2</sub> for 1 hour prior to the inoculation. To investigate the oxygen tolerance of *S. ovata*, the *S. ovata* was grown in a micro-aerobic condition containing 4% O<sub>2</sub> (N<sub>2</sub>:CO<sub>2</sub>:O<sub>2</sub> = 76:20:4). The inoculated serum vials were kept in a shaking incubator (Incu-Shake MIDI SciQuip; 303 K, 180 rpm) for 6 days. The growth of *S. ovata* was monitored by measuring CH<sub>3</sub>COO<sup>-</sup> concentration (Supplementary Fig. 16) using <sup>1</sup>H NMR (Bruker 400 MHz) and trimethylsilylpropanoic acid (TSP) as the internal standard in D<sub>2</sub>O as well as optical density at 600 nm using a UV-Vis spectrometer (Varian Cary 50, Agilent Technologies).

### **Culturing of *G. sulfurreducens***

*G. sulfurreducens* PCA (ATCC 51573) was purchased from DSMZ-German Collection of Microorganisms and Cell Cultures GmbH (DSM No.: 12127). *G. sulfurreducens* cells were grown with sodium acetate (20 mM, Sigma-Aldrich, anhydrous, for molecular biology,  $\geq 99\%$ ) as the electron donor and sodium fumarate dibasic (50 mM, Sigma-Aldrich,  $\geq 99\%$ ) as the electron acceptor in the DSMZ-recommended growth medium (DSMZ 826) (Supplementary Table 5). The medium was purged with 20%CO<sub>2</sub>/80%N<sub>2</sub> for 1 hour before the inoculation. The inoculated serum vials were kept in a shaking incubator (303 K, 180 rpm) for 6 days. The concentration of bacterial suspension was determined by measuring optical density at 600 nm using the UV-vis spectrometer.

#### **Preparation of SrTiO<sub>3</sub>:La,Rh|ITO|BiVO<sub>4</sub>:Mo photocatalyst sheets**

A two-step solid-state reaction was used to synthesise SrTiO<sub>3</sub>:La,Rh (La/(La + Sr) = Rh/(Rh + Ti) = 4 mol%) according to a previously reported procedure.<sup>19</sup> SrCO<sub>3</sub> (Alfa Aesar, 99.99%) and rutile TiO<sub>2</sub> (Sigma-Aldrich,  $\geq 99.98\%$ ) powders (Sr/Ti = 1.05) were mixed in a mortar, followed by calcination in an alumina crucible at 1473 K for 10 h. Subsequently, La<sub>2</sub>O<sub>3</sub> (Fisher Scientific, 99.99%) and Rh<sub>2</sub>O<sub>3</sub> (Wako Pure Chemical, 98.0–102.0%) were added into the resulting SrTiO<sub>3</sub> and heated at 1373 K for 6 h.

BiVO<sub>4</sub>:Mo (Mo/V = 0.05 mol%) was synthesised through aqueous processes.<sup>19</sup> A layered Mo-doped K<sub>3</sub>V<sub>5</sub>O<sub>14</sub> was first obtained by calcining the mixture of K<sub>2</sub>CO<sub>3</sub> (Breckland Scientific, 99.5%), V<sub>2</sub>O<sub>5</sub> (Fisher Scientific, 99.6%), and MoO<sub>3</sub> (Mo/V = 0.05 mol%, BDH Chemicals, 99.5%) in air at 723 K for 5 h. Stoichiometric Bi(NO<sub>3</sub>)<sub>3</sub>·5H<sub>2</sub>O (Sigma-Aldrich, 98%) was added to 100 mL distilled water to form a suspension of BiONO<sub>3</sub>. The resulting Mo-doped K<sub>3</sub>V<sub>5</sub>O<sub>14</sub> was added to the BiONO<sub>3</sub> suspension and stirred mildly at 343 K for 10 h. The obtained powder was collected by filtration, washed with distilled water, and then dried overnight in air before use.



SrTiO<sub>3</sub>:La,Rh|ITO|BiVO<sub>4</sub>:Mo photocatalyst sheets were prepared by a drop-casting method. A mixture of SrTiO<sub>3</sub>:La,Rh, BiVO<sub>4</sub>:Mo powders (2.5 mg each), and ITO nanoparticles (Sigma-Aldrich, average size 30 nm; 1.2 mg) was suspended in isopropanol (Sigma-Aldrich, ≥99.5%, 0.25 mL) by ultrasonication for 30 min and then drop-cast on a glass substrate (ca. 1.5 cm × 1.5 cm). The obtained sheet was dried in air at room temperature. The SrTiO<sub>3</sub>:La,Rh|ITO|BiVO<sub>4</sub>:Mo sheet was obtained after annealing in air at 573 K for 30 min.

### **Cocatalyst loading on the photocatalyst sheet**

The photocatalyst sheets were modified with nanoparticulate Ru species by photodeposition.<sup>19</sup> The photodeposition reactions were conducted in a closed system with side illumination from a 150 W Xe lamp (Newport Oriel 6255;  $\lambda > 200$  nm) with an infrared water filter. The photocatalyst sheet samples (~2.2 cm<sup>2</sup>) were attached to a steel rod and inserted into the reaction cell. In the initial step, Ru species were photodeposited on the photocatalyst sheets from RuCl<sub>3</sub> (Acros Organics, 35–40% ruthenium) dissolved in distilled water (35 ml). Subsequently, the reactant was changed to an aqueous K<sub>2</sub>CrO<sub>4</sub> solution (Sigma-Aldrich, ≥99 %) and a thin Cr<sub>2</sub>O<sub>3</sub> layer was coated on metallic Ru nanoparticles on the surface of SrTiO<sub>3</sub>:La,Rh by photodeposition.<sup>19,39</sup> The amounts of RuCl<sub>3</sub> and K<sub>2</sub>CrO<sub>4</sub> were 0.3 and 0.15 μmol for a photocatalyst sheet sample 2.2 cm<sup>2</sup> in size. Before performing the photodeposition reaction, the reactant in the cell was purged for 30 min with N<sub>2</sub> containing 2% CH<sub>4</sub> as an internal standard for gas chromatography measurements. The pH of the reactant after N<sub>2</sub> purging was 6.9. The photodeposition was monitored by measuring produced amounts of H<sub>2</sub> and O<sub>2</sub>. The photodeposition was finished when the gas evolution rates became steady, typically 10 and 6 hours for Ru and Cr<sub>2</sub>O<sub>3</sub> deposition, respectively.

For the experiments without loading of Cr<sub>2</sub>O<sub>3</sub>/Ru as H<sub>2</sub> evolution cocatalyst on the photocatalyst sheet, RuO<sub>2</sub> (1 wt%) was loaded on BiVO<sub>4</sub>:Mo particles in advance of the sheet preparation by an

impregnation method.<sup>32</sup> BiVO<sub>4</sub>:Mo powder (0.1–0.2 g) was put in an evaporating dish. After adding an aqueous solution containing a given amount of RuCl<sub>3</sub>, the evaporating dish was placed in a water bath. The powder was collected and calcined in air at 623 K for 1 h when the solution was evaporated to dryness.

### **Fabrication of photoelectrodes**

The IO-ITO electrode was prepared by a previously reported co-assembly method.<sup>40</sup> Initially, ITO nanoparticles (Sigma-Aldrich, average size < 50 nm; 20 mg) were added into a mixture of methanol and water (11:1 v:v; 125  $\mu$ L) and sonicated for 3 h. Polystyrene (PS) latex (Polysciences Inc.; 10  $\mu$ m, 0.75 mL, 2.5 wt% in water) was centrifuged at 10,000 rpm for 3 min to remove the supernatant. The ITO nanoparticles dispersion was mixed with the PS beads and sonicated for 30 min in ice water (< 277 K) to obtain a uniform mixture. The PS-ITO mixture (15  $\mu$ L) was drop-casted onto an ITO glass slide (Visiontek System Ltd.; 1 cm  $\times$  2.5 cm  $\times$  0.11 cm, 12  $\Omega$  cm<sup>-2</sup>) with a pre-defined area of 0.25 cm<sup>2</sup>, and kept drying in air for 30 min. The IO-ITO electrodes were obtained by annealing the glass slides at 773 K in air for 20 min at a ramping rate of 1 K min<sup>-1</sup> from room temperature. The thickness of the IO-ITO scaffold was  $\sim$ 60  $\mu$ m (Supplementary Fig. 17b). Copper wires were embedded in indium at the bottom of the sample to establish electrical contact. The copper wire and indium were encapsulated with epoxy (Araldite, Rapid 5-Minute Epoxy).

### **Characterisation**

The diffuse-reflectance spectra were obtained using an ultraviolet-visible-near-infrared spectrometer (Varian Cary 50 Bio). A TESCAN MIRA3 FEG-SEM instrument with an Oxford Instruments Aztec Energy X-maxN 80 system was used to collect the SEM and SEM-EDX element mapping images at an acceleration voltage of 5 and 15 kV, respectively. X-ray diffraction patterns of

the samples were measured with a PANalytical Empyrean Series 2 instrument using Cu K $\alpha$  source operated at 40 kV and 40 mA. ICP-OES measurements were carried out on a Thermo Scientific iCAP 7400 ICP-OES DUO spectrometer. Analyte solutions for ICP-OES were obtained by digesting the sheets in aqueous HNO<sub>3</sub> (>68%) for one day and dilution to 2% vol/vol with Milli-Q water.

### **Protein quantification**

The protein concentrations were quantified with the Bio-Rad protein assay (Bio-Rad Protein Assay Kit #5000002) as previously reported.<sup>62</sup> Bacteria attached on the photocatalyst sheet were dipped in a sodium dodecyl solution (5 mL, 10 wt%) solution at 372 K for 15 min to extract proteins from the sample. The solution was centrifuged (14,000 rpm, 10 min) to remove the impurities. The supernatant was then collected to quantify the protein by the Bio-Rad protein assay utilising the principle of protein-dye binding. 5 mL of the diluted dye reagent, which was incubated at 298 K for 10 min, was added in a clean vial containing the protein solution (100  $\mu$ L). The absorbance of the solution at 600 nm was measured using the UV-vis spectrometer. Bovine serum albumin was used as the protein standard to make the correlation curve and the protein concentration was calculated from the standard curve.

### **Photocatalytic reactions**

The photocatalytic reactions were performed in a closed system with side illumination from Newport Oriel 67005 solar light simulators (150 W, 100 mW cm<sup>-2</sup> across the solar spectrum, AM 1.5 G,  $\lambda > 200$  nm) with infrared water filter, which were calibrated using a certified Newport 1916-R optical power meter. The photocatalyst sheet samples (ca. 2.2 cm<sup>2</sup>) were attached to a steel rod and inserted into the reaction cell containing an *S. ovata* medium (DSMZ 311) without betaine, Naresazurin solution, casitone, L-cysteine, yeast extract, and Na<sub>2</sub>S (Supplementary Table 2) (12 mL)

unless otherwise noted. Before conducting the CO<sub>2</sub>RR, the reactant in the cell was purged for 40 min with the mixture of N<sub>2</sub> and CO<sub>2</sub> (N<sub>2</sub>:CO<sub>2</sub> = 80:20), unless otherwise noted. The betaine-grown *S. ovata* cells were then injected into the reactor (final optical density at 600 nm: 0.6) and purged with the same gas mixture for another 20 minutes. The pH of the medium after purging was 7.0.

The sheet and bacteria separated system (Figure 2b) employed the photocatalyst sheet in a separate compartment from *S. ovata* with the headspace connecting the two chambers. The two chambers contained the same reaction medium purged with the mixture of N<sub>2</sub> and CO<sub>2</sub> (N<sub>2</sub>:CO<sub>2</sub> = 80:20), as mentioned above.

In the 45-h photosynthetic reaction, Cr<sub>2</sub>O<sub>3</sub> was reloaded every 15 h. The photocatalyst sheet was taken out of the reaction medium after the first run and put in a fresh reaction medium added with 0.15 μmol K<sub>2</sub>CrO<sub>4</sub>. The photodeposition was carried out for 3 h under a 150 W Xe lamp irradiation. The photocatalyst sheet was then inserted in another new reaction medium to start the second run. The reactant was purged for 40 min with the mixture of N<sub>2</sub> and CO<sub>2</sub> (N<sub>2</sub>:CO<sub>2</sub> = 80:20). The *S. ovata* cells obtained from the reaction medium in the first run by centrifugation were then injected into the reactor and purged with the same gas mixture for another 20 minutes. Subsequently, the reaction was restarted by exposing to the simulated sunlight illumination (AM 1.5G, 100 mW cm<sup>-2</sup>).

The water-splitting reaction using the Cr<sub>2</sub>O<sub>3</sub>/Ru-SrTiO<sub>3</sub>:La,Rh|ITO|RuO<sub>2</sub>-BiVO<sub>4</sub>:Mo photocatalyst sheet in the absence of *S. ovata* was carried out in the same reaction medium purging with N<sub>2</sub> containing 2% CH<sub>4</sub> as an internal standard for gas chromatography measurements.

In the colloidal systems for photocatalytic CO<sub>2</sub>RR over *S. ovata*|RuO<sub>2</sub>-BiVO<sub>4</sub>:Mo, RuO<sub>2</sub>-BiVO<sub>4</sub>:Mo powder (2 mg) was dispersed in an *S. ovata* medium (2 mL) in Pyrex glass photoreactor vials capped with rubber septa. The samples were purged with a mixture of N<sub>2</sub> and CO<sub>2</sub> (N<sub>2</sub>:CO<sub>2</sub> = 80:20) for 40 min. After injecting the betaine-grown *S. ovata* cells, the reactor was purged with the same gas mixture for another 20 min. For the H<sub>2</sub> evolution reaction over SrTiO<sub>3</sub>:La,Rh in the presence

of  $\text{CH}_3\text{COO}^-$ ,  $\text{SrTiO}_3\text{:La,Rh}$  powder (2 mg) was added to an aqueous solution of  $\text{CH}_3\text{COONa}$  (18 mM, 2 mL). After briefly vortexing, the samples were purged with  $\text{N}_2$  containing 2%  $\text{CH}_4$  as an internal standard at ambient pressure for 40 min. The above reactions were carried out under simulated sunlight irradiation (AM 1.5G,  $100 \text{ mW cm}^{-2}$ ).

### Products quantification

Concentrations of  $\text{CH}_3\text{COO}^-$  were measured by  $^1\text{H}$  NMR spectroscopy (Bruker 400 MHz) with trimethylsilylpropanoic acid (TSP) as the internal standard in  $\text{D}_2\text{O}$ . Spectra were processed using the Bruker TopSpin Software. A Shimadzu GC-2010 Plus gas chromatograph equipped with a barrier discharge ionisation detector was used to quantify  $\text{H}_2$ . The GC-2010 Plus was equipped with Hayesep D (2 m \* 1/8'' OD \* 2 mm ID, 80/100 mesh, Analytical Columns) pre-column and a RT-Molsieve 5A (30 m \* 0.53 mm ID, Restek) main column. Aliquots (50  $\mu\text{L}$ ) of the headspace gas were collected from the sealed cell using a gastight syringe (Hamilton, GASTIGHT 1710) for gas chromatography analysis. The  $\text{O}_2$  quantification was performed in a glovebox ( $\text{O}_2$  concentration < 3 ppm) using a NeoFox-GT fluorometer and Fospor-R fluorescence oxygen sensor probe from Ocean Optics. The analytical errors are <5% for quantifying  $\text{H}_2$  and <10% for  $\text{O}_2$ .

### Isotopic labelling

The photosynthetic reaction over  $S. ovata|\text{Cr}_2\text{O}_3/\text{Ru-SrTiO}_3\text{:La,Rh}|\text{ITO}|\text{RuO}_2\text{-BiVO}_4\text{:Mo}$  hybrid system was performed in a reaction medium containing 47 mM  $\text{NaH}^{13}\text{CO}_3$  (Sigma-Aldrich, 98 atom%  $^{13}\text{C}$ , 99% (CP)) with the mixture of  $\text{N}_2$  and  $^{13}\text{CO}_2$  (Sigma-Aldrich, 99.0 atom %  $^{13}\text{C}$ , 99% (CP);  $\text{N}_2\text{:}^{13}\text{CO}_2 = 80\text{:}20$ ) as the headspace gas. The amounts of  $\text{CH}_3\text{COO}^-$  produced in 5 and 15 h were analysed by  $^1\text{H}$  NMR and  $^{13}\text{C}$  NMR spectroscopy conducted on a Bruker 400 MHz spectrometer.

### Quantum yield measurements

The AQY of the photosynthetic reaction was calculated using

$$\text{AQY} = (16R/I) \times 100\% \quad (6)$$

Where  $R$  and  $I$  denote the  $\text{CH}_3\text{COO}^-$  production rate and the photon flux of monochromatic light, respectively. To form one acetate molecule, eight electrons in  $\text{SrTiO}_3:\text{La,Rh}$  must be consumed in the  $\text{CO}_2\text{RR}$ . Meanwhile, eight electrons in  $\text{BiVO}_4:\text{Mo}$  must be combined with the holes in  $\text{SrTiO}_3:\text{La,Rh}$ . Sixteen electrons are therefore required to produce one acetate molecule. The AQYs were determined using a LOT MSH-300 monochromator. Thorlabs PM100D power meter and Thorlabs S302C thermal power sensor were used to measure power at different wavelengths. The wavelength  $\lambda$  with a full width at half maximum of 15 nm was varied between 390 and 540 nm in 30 nm steps.

### Solar-to-acetate (STA) conversion efficiency

The STA is given as

$$\text{STA} (\%) = (R(\text{CH}_3\text{COO}^-) \times \Delta G_r) / (P \times S) \times 100 \quad (7)$$

where  $R(\text{CH}_3\text{COO}^-)$ ,  $\Delta G_r$ ,  $P$ , and  $S$  indicate the rate of  $\text{CH}_3\text{COO}^-$  formation during the photosynthetic reaction, the energy intensity of the AM 1.5G solar irradiation ( $100 \text{ mW cm}^{-2}$ ) and the irradiated sample area, respectively.

### Microbial electrogenesis

The  $\text{CH}_3\text{COO}^-$  (~9 mM; 15 mL) produced by *S. ovata*| $\text{Cr}_2\text{O}_3/\text{Ru-SrTiO}_3:\text{La,Rh}$ |ITO| $\text{RuO}_2\text{-BiVO}_4:\text{Mo}$  hybrid system via a 15 h photosynthetic reaction was used as feedstock and electrolyte to generate electricity using *G. sulfurreducens* as the model electric bacterium. The microbial electrogenesis on *G. sulfurreducens*|IO-ITO electrode ( $0.25 \text{ cm}^2$ ) was performed in a three-electrode configuration using a Ag/AgCl reference electrode (in saturated NaCl aqueous solution, Basi MW-

2030) and a platinum mesh counter electrode. The solution obtained from the photosynthetic reaction was purged with a mixture of N<sub>2</sub> and CO<sub>2</sub> (N<sub>2</sub>:CO<sub>2</sub> = 80:20) for 40 minutes. The freshly grown *G. sulfurreducens* was inoculated into the reactor (final optical density at 600 nm: 0.6) and purged for another 20 minutes. The reactor was kept at constant temperature (303 K) and stirring (200 rpm). The working electrode was poised with a potential of 0.1 V vs SHE using a potentiostat (MultiEmStat3+).

### **Statistics and Reproducibility**

The mean values and standard deviations of data sets are calculated using the AVERAGE and STDEV.S function of Microsoft Excel (Microsoft 365), respectively. Regarding the SEM and SEM-EDX element mapping images, two to five distinct locations with similar morphologies were captured for each sample and representative images are shown.

### **Data availability**

All source data that support the findings of this study are available from the University of Cambridge data repository: <https://doi.org/10.17863/CAM.84871>.

### **Acknowledgements**

We thank Dr Motiar Rahaman, Dr Lin Su, and Miss Melanie Miller (University of Cambridge) for helpful discussions and Dr Heather Greer at the University of Cambridge for assisting in the collection of SEM-EDX element mapping images. This work was supported by a European Research Council (ERC) Consolidator Grant ‘MatEnSAP’ (682833 to E.R.), UK Research and Innovation Cambridge Creative Circular Plastics Centre (grant EP/S025308), European Marie Skłodowska-Curie individual Fellowships (to Q.W., GAN 793996 and to S.K., GAN 744317), Research England’s Expanding

Excellence in England (E3) Fund (to S.K.), the Cambridge Trust (Cambridge Thai Foundation Award to C.P.) and a Trinity-Henry Barlow Scholarship (to C.P.).

### Author contributions

Q.W., S.K., and E.R. conceived the idea and designed the project. Q.W. prepared the photocatalyst sheet and photoelectrodes and conducted physical characterisations of the semiconductors. S.K. and Q.W. carried out the bacteria culturing. S.K. quantified the protein and performed the microbial electrogenesis. C.P. recorded the SEM and SEM-EDX element mapping images. Q.W. and C.P. carried out H<sub>2</sub> and O<sub>2</sub> qualification. S.K., C.D.S., and C.P. quantified acetate. The O<sub>2</sub>-tolerance ability of bacteria was investigated by C.D.S. and S.K. C.D.S., S.K., and Q.W. conducted the isotopic labelling experiments. All authors analysed the data and discussed the results. Q.W., S.K., and E.R. wrote the manuscript with assistance from the other co-authors. E.R. supervised the project.

### Competing interests

The authors declare no competing interests.

**Figure 1 | *S. ovata*|sheet hybrid system. a**, Mechanistic pathway diagram depicting the photosynthetic CO<sub>2</sub>-to-acetate conversion coupled with water oxidation over *S. ovata*|Cr<sub>2</sub>O<sub>3</sub>/Ru-SrTiO<sub>3</sub>:La,Rh|ITO|RuO<sub>2</sub>-BiVO<sub>4</sub>:Mo. CB and VB indicate conduction band and valence band, respectively. M<sub>ox</sub> and M<sub>red</sub> represent intracellular oxidized and reduced redox mediators, respectively. *hν* indicates light irradiation. The conduction and valence band potentials for SrTiO<sub>3</sub>:La,Rh are located at -0.9 and +2.3 V vs. NHE at pH 7, respectively.<sup>36</sup> The visible light absorption ability of SrTiO<sub>3</sub>:La,Rh is assigned to photoexcitation from the donor levels formed by Rh<sup>3+</sup> ions (+1.7 vs. NHE at pH 7) to its conduction band. BiVO<sub>4</sub>:Mo has a conduction band and valence band potential



of  $-0.3$  and  $+2.1$  V vs. NHE at pH 7, respectively.<sup>45</sup> The reduction potential of  $H^+/H_2$  and  $O_2/H_2O$  is  $-0.41$  and  $+0.82$  V (vs. NHE at pH 7), respectively. The reduction potential of  $CO_2/CH_3COO^-$  ( $-0.3$  vs. NHE at pH 7) was determined by the reaction Gibbs energy of the  $CO_2$ -to- $CH_3COO^-$  conversion coupled with water oxidation ( $873$  kJ mol<sup>-1</sup> at 1 atm and 298 K).<sup>14</sup> **b-c**, Photographs of  $1.5$  cm  $\times$   $1.5$  cm  $Cr_2O_3/Ru-SrTiO_3:La,Rh|ITO|RuO_2-BiVO_4:Mo$  photocatalyst sheets before (**b**) and after (**c**) 15 h photosynthetic reaction.

**Figure 2 | Photosynthetic activity of the *S. ovata*/sheet hybrids.** **a**, Time course of the photosynthetic  $CH_3COO^-$ ,  $O_2$  and  $H_2$  production over  $S. ovata|Cr_2O_3/Ru-SrTiO_3:La,Rh|ITO|RuO_2-BiVO_4:Mo$  hybrids. Error bars correspond to the standard deviation ( $n = 3$  independent samples). The open circles and solid circles indicate the individual data points and mean values, respectively. The light blue area represents the standard deviation for  $O_2$  evolution. The red and purple vertical lines represent the standard deviation for  $CH_3COO^-$  and  $H_2$ , respectively. The dashed lines are guides to the eye. **b**, Time course of the  $CH_3COO^-$ ,  $O_2$  and  $H_2$  production over a system separated the photocatalyst sheet and *S. ovata* into two chambers. Error bars correspond to the standard deviation ( $n = 2$  independent samples). The open circles and solid circles indicate the individual data points and mean values, respectively. The light blue area represents the standard deviation for  $O_2$  evolution. The red and purple vertical lines represent the standard deviation for  $CH_3COO^-$  and  $H_2$ , respectively. The dashed lines are guides to the eye. **c**, Dependence of AQY for  $CH_3COO^-$  production on incident light wavelength, along with diffuse reflectance spectra of  $SrTiO_3:La,Rh$  (red dashed line), and  $BiVO_4:Mo$  (red line) for comparison. The blue dots indicate the AQYs of the system at various incident light wavelengths. The full width at half maximum of incident wavelength is 15 nm. F(R), Kubelka–Munk function. **d**,  $^1H$  NMR spectra ( $D_2O$ , 400 MHz) of the solution after 5 and 15 h of irradiation using  $^{12}CO_2/H^{12}CO_3^-$  (yellow and orange trace, respectively) and  $^{13}CO_2/H^{13}CO_3^-$  (light green and dark green

trace, respectively) as the carbon sources. The reactions were carried out in a reaction medium purged with 80%N<sub>2</sub>:20%CO<sub>2</sub> (pH 7.0) under ambient conditions (298 K, 1 atm) and 1 sun illumination (AM 1.5G, 100 mW cm<sup>-2</sup>).

**Figure 3 | Morphology of *S. ovata*|sheet hybrids.** **a**, Top-view SEM image of a *S. ovata*|Cr<sub>2</sub>O<sub>3</sub>/Ru-SrTiO<sub>3</sub>:La,Rh|ITO|RuO<sub>2</sub>-BiVO<sub>4</sub>:Mo sheet after 15 h photosynthetic reaction over the hybrid system. **b-e**, Top-view SEM-EDX elemental mapping images of a *S. ovata*|Cr<sub>2</sub>O<sub>3</sub>/Ru-SrTiO<sub>3</sub>:La,Rh|ITO|RuO<sub>2</sub>-BiVO<sub>4</sub>:Mo sheet after 15 h photosynthetic reaction over the hybrid system, showing a superimposition (**b**) of the distributions of Sr (**c**), Bi (**d**) and In (**e**).

**Figure 4 | Viability of the *S. ovata*|sheet hybrids.** **a**, Products accumulation for 3 runs of 15 hours, with the reloading of Cr<sub>2</sub>O<sub>3</sub> on the *S. ovata*|Cr<sub>2</sub>O<sub>3</sub>/Ru-SrTiO<sub>3</sub>:La,Rh|ITO|RuO<sub>2</sub>-BiVO<sub>4</sub>:Mo hybrid and replenishing the reactant medium with a fresh solution and 80%N<sub>2</sub>/20%CO<sub>2</sub> purging every 15 hours. The sample areas were ~2.2 cm<sup>2</sup>. Error bars correspond to the standard deviation (n = 3 independent samples). The bars show the mean values and the black vertical lines indicate the standard deviation. The open circles represent the individual data points. **b**, Dependence of the photosynthetic activity of the *S. ovata*|Cr<sub>2</sub>O<sub>3</sub>/Ru-SrTiO<sub>3</sub>:La,Rh|ITO|RuO<sub>2</sub>-BiVO<sub>4</sub>:Mo hybrid system on the CO<sub>2</sub> concentration in the headspace. Error bars correspond to the standard deviation (n = 2 independent samples). The bars show the mean values and the black vertical lines indicate the standard deviation. The open circles represent the individual data points. The reactions were carried out in a reaction medium purged with 80%N<sub>2</sub>:20%CO<sub>2</sub> (pH 7.0) under ambient conditions (298 K, 1 atm) and 1 sun illumination (AM 1.5G, 100 mW cm<sup>-2</sup>).

**Figure 5 | *G. sulfurreducens*|IO-ITO electrode producing electricity.** **a**, Schematic diagram showing that the sunlight-driven *S. ovata*|Cr<sub>2</sub>O<sub>3</sub>/Ru-SrTiO<sub>3</sub>:La,Rh|ITO|RuO<sub>2</sub>-BiVO<sub>4</sub>:Mo hybrid provides a biohybrid electrochemical system with CH<sub>3</sub>COO<sup>-</sup> to realise the current generation and close the carbon cycle. IO-ITO represents porous inverse opal-ITO electrode. **b**, Current production by *G. sulfurreducens*|IO-ITO electrode at 0.1 V vs. SHE with CH<sub>3</sub>COO<sup>-</sup> (ca. 9 mM; pH 7.2, 303 K), which was produced in 15 h by the *S. ovata*|Cr<sub>2</sub>O<sub>3</sub>/Ru-SrTiO<sub>3</sub>:La,Rh|ITO|RuO<sub>2</sub>-BiVO<sub>4</sub>:Mo hybrid system under simulated sunlight irradiation (AM 1.5G, 100 mW cm<sup>-2</sup>). Error bars correspond to the standard deviation (n = 3 independent samples). The red circles indicate the mean values and the light red area represents the standard deviation.

## References

1. Jiang, K. *et al.* Metal ion cycling of Cu foil for selective C–C coupling in electrochemical CO<sub>2</sub> reduction. *Nat. Catal.* **1**, 111–119 (2018).
2. Morales-Guio, C. G. *et al.* Improved CO<sub>2</sub> reduction activity towards C<sub>2+</sub> alcohols on a tandem gold on copper electrocatalyst. *Nat. Catal.* **1**, 764–771 (2018).
3. Nitopi, S. *et al.* Progress and perspectives of electrochemical CO<sub>2</sub> reduction on copper in aqueous electrolyte. *Chem. Rev.* **119**, 7610–7672 (2019).
4. García de Arquer, F. P. *et al.* CO<sub>2</sub> electrolysis to multicarbon products at activities greater than 1 A cm<sup>-2</sup>. *Science* **367**, 661–666 (2020).
5. Rahaman, M., Dutta, A., Zanetti, A. & Broekmann, P. Electrochemical reduction of CO<sub>2</sub> into multicarbon alcohols on activated Cu mesh catalysts: an identical location (IL) study. *ACS Catal.* **7**, 7946–7956 (2017).

6. Birdja, Y. Y. *et al.* Advances and challenges in understanding the electrocatalytic conversion of carbon dioxide to fuels. *Nat. Energy* **4**, 732–745 (2019).
7. Claassens, N. J., Sousa, D. Z., dos Santos, V. A. P. M., de Vos, W. M. & van der Oost, J. Harnessing the power of microbial autotrophy. *Nat. Rev. Microbiol.* **14**, 692–706, (2016).
8. Lapinsonnière, L., Picot, M. & Barrière, F. Enzymatic versus microbial bio-catalyzed electrodes in bio-electrochemical systems. *ChemSusChem* **5**, 995–1005 (2012).
9. Cestellos-Blanco, S., Zhang, H., Kim, J. M., Shen, Y.-x. & Yang, P. Photosynthetic semiconductor biohybrids for solar-driven biocatalysis. *Nat. Catal.* **3**, 245–255 (2020).
10. Kornienko, N., Zhang, J. Z., Sakimoto, K. K., Yang, P. & Reisner, E. Interfacing nature's catalytic machinery with synthetic materials for semi-artificial photosynthesis. *Nat. Nanotechnol.* **13**, 890–899 (2018).
11. Bian, B., Bajracharya, S., Xu, J., Pant, D. & Saikaly, P. E. Microbial electrosynthesis from CO<sub>2</sub>: Challenges, opportunities and perspectives in the context of circular bioeconomy. *Bioresour. Technol.* **302**, 122863 (2020).
12. Li, H. *et al.* Integrated electromicrobial conversion of CO<sub>2</sub> to higher alcohols. *Science* **335**, 1596–1596 (2012).
13. Haas, T., Krause, R., Weber, R., Demler, M. & Schmid, G. Technical photosynthesis involving CO<sub>2</sub> electrolysis and fermentation. *Nat. Catal.* **1**, 32–39 (2018).
14. Liu, C. *et al.* Nanowire–Bacteria hybrids for unassisted solar carbon dioxide fixation to value-added chemicals. *Nano Lett.* **15**, 3634–3639 (2015).
15. Nichols, E. M. *et al.* Hybrid bioinorganic approach to solar-to-chemical conversion. *Proc. Natl. Acad. Sci. U. S. A.* **112**, 11461–11466 (2015).

16. Liu, C., Colón, B. C., Ziesack, M., Silver, P. A. & Nocera, D. G. Water splitting–biosynthetic system with CO<sub>2</sub> reduction efficiencies exceeding photosynthesis. *Science* **352**, 1210–1213 (2016).
17. Sakimoto, K. K., Zhang, S. J. & Yang, P. Cysteine–cystine photoregeneration for oxygenic photosynthesis of acetic acid from CO<sub>2</sub> by a tandem inorganic–biological hybrid system. *Nano Lett.* **16**, 5883–5887 (2016).
18. Su, Y. *et al.* Close-packed nanowire-bacteria hybrids for efficient solar-driven CO<sub>2</sub> fixation. *Joule*, **4**, 800–811 (2020).
19. Wang, Q. *et al.* Scalable water splitting on particulate photocatalyst sheets with a solar-to-hydrogen energy conversion efficiency exceeding 1%. *Nat. Mater.* **15**, 611–615 (2016).
20. Geisz, J. F. *et al.* Six-junction III–V solar cells with 47.1% conversion efficiency under 143 Suns concentration. *Nat. Energy* **5**, 326–335 (2020).
21. Yoshikawa, K. *et al.* Silicon heterojunction solar cell with interdigitated back contacts for a photoconversion efficiency over 26%. *Nat. Energy* **2**, 17032 (2017).
22. Ager, J. W., Shaner, M. R., Walczak, K. A., Sharp, I. D. & Ardo, S. Experimental demonstrations of spontaneous, solar-driven photoelectrochemical water splitting. *Energy Environ. Sci.* **8**, 2811–2824 (2015).
23. Ardo, S. *et al.* Technical and economic feasibility of centralized facilities for solar hydrogen production via photocatalysis and photoelectrochemistry. *Energy Environ. Sci.* **6**, 1983–2002 (2013).
24. Pinaud, B. A. *et al.* Technical and economic feasibility of centralized facilities for solar hydrogen production via photocatalysis and photoelectrochemistry. *Energy Environ. Sci.* **6**, 1983–2002 (2013).

25. Gai, P. *et al.* Solar-powered organic semiconductor–bacteria biohybrids for CO<sub>2</sub> reduction into acetic acid. *Angew. Chem. Int. Ed.* **59**, 7224–7229 (2020).
26. Sakimoto, K. K., Wong, A. B. & Yang, P. Self-photosensitization of nonphotosynthetic bacteria for solar-to-chemical production. *Science* **351**, 74–77 (2016).
27. Zhang, H. *et al.* Bacteria photosensitized by intracellular gold nanoclusters for solar fuel production. *Nat. Nanotechnol.* **13**, 900–905 (2018).
28. Göbbels, L. *et al.* Cysteine: an overlooked energy and carbon source. *Sci. Rep.* **11**, 2139 (2021).
29. Kaden, J., S. Galushko, A. & Schink, B. Cysteine-mediated electron transfer in syntrophic acetate oxidation by cocultures of *Geobacter sulfurreducens* and *Wolinella succinogenes*. *Arch. Microbiol.* **178**, 53–58 (2002).
30. Liu, D., Dong, H., Zhao, L. & Wang, H. Smectite reduction by *Shewanella* species as facilitated by cystine and cysteine. *Geomicrobiol. J.* **31**, 53–63 (2014).
31. Zhu, S. & Wang, D. Photocatalysis: Basic principles, diverse forms of implementations and emerging scientific opportunities. *Adv. Energy Mater.* **7**, 1700841 (2017).
32. Wang, Q. *et al.* Molecularly engineered photocatalyst sheet for scalable solar formate production from carbon dioxide and water. *Nat. Energy*, **5**, 703–710 (2020).
33. Wang, Q. *et al.* Z-scheme water splitting using particulate semiconductors immobilized onto metal layers for efficient electron relay. *J. Catal.* **328**, 308–315 (2015).
34. Li, X., Yu, J. Jaroniec, M. & Chen, X. Cocatalysts for selective photoreduction of CO<sub>2</sub> into solar fuels. *Chem. Rev.* **119**, 3962–4179 (2019).
35. Nevin, K. P., Woodard, T. L., Franks, A. E., Summers, Z. M. & Lovley, D. R. Microbial electrosynthesis: feeding microbes electricity to convert carbon dioxide and water to multicarbon extracellular organic compounds. *mBio* **1**, e00103–00110 (2010).

36. Moss, B. *et al.* Linking in situ charge accumulation to electronic structure in doped SrTiO<sub>3</sub> reveals design principles for hydrogen-evolving photocatalysts. *Nat. Mater.* **20**, 511–517 (2021).
37. Wang, Q. *et al.* Printable photocatalyst sheets incorporating a transparent conductive mediator for Z-scheme water splitting. *Joule* **2**, 2667–2680 (2018).
38. Ebihara, M. *et al.* Charge carrier mapping for Z-scheme photocatalytic water-splitting sheet via categorization of microscopic time-resolved image sequences. *Nat. Commun.* **12**, 3716 (2021).
39. Maeda, K. *et al.* Noble-Metal/Cr<sub>2</sub>O<sub>3</sub> core/shell nanoparticles as a cocatalyst for photocatalytic overall water splitting. *Angew. Chem. Int. Ed.* **45**, 7806–7809 (2006).
40. Fang, X., Kalathil, S., Divitini, G., Wang, Q. & Reisner, E. A three-dimensional hybrid electrode with electroactive microbes for efficient electrogenesis and chemical synthesis. *Proc. Natl. Acad. Sci. U. S. A.* **117**, 5074–5080 (2020).
41. Cerdan, S., Künnecke, B. & Seelig, J. Cerebral metabolism of [1,2-<sup>13</sup>C<sub>2</sub>]acetate as detected by in vivo and in vitro <sup>13</sup>C NMR. *J. Biol Chem.* **265**, 12916–12926 (1990).
42. Wasylenko, T. M. & Stephanopoulos, G. Kinetic isotope effects significantly influence intracellular metabolite <sup>13</sup>C labeling patterns and flux determination. *Biotechnol. J.* **8**, 1080–1089 (2013).
43. Millard, P., Portais, J.-C. & Mendes, P. Impact of kinetic isotope effects in isotopic studies of metabolic systems. *BMC Syst. Biol.* **9**, 1–13 (2015).
44. Morello, G., Megarity, C. F. & Armstrong, F. A. The power of electrified nanoconfinement for energising, controlling and observing long enzyme cascades. *Nat. Commun.* **12**, 340 (2021).
45. Kudo, A., Omori, K. & Kato, A novel aqueous process for preparation of crystal form-controlled and highly crystalline BiVO<sub>4</sub> powder from layered vanadates at room temperature and its photocatalytic and photophysical properties. *J. Am. Chem. Soc.* **121**, 11459–11467 (1999).

46. Lyu, H. *et al.* An Al-doped SrTiO<sub>3</sub> photocatalyst maintaining sunlight-driven overall water splitting activity for over 1000 h of constant illumination. *Chem. Sci.* **10**, 3196–3201 (2019).
47. Lu, Z. & Imlay, J. A. When anaerobes encounter oxygen: mechanisms of oxygen toxicity, tolerance and defence. *Nat. Rev. Microbiol.* **19**, 774–785 (2021).
48. Jenney, F. E., Verhagen, M. F. J. M., Cui, X. & Adams, M. W. W. Anaerobic microbes: oxygen detoxification without superoxide dismutase. *Science* **286**, 306–309 (1999).
49. Nakanishi, T., Inoue, H. & Kitamura, M. Cloning and expression of the superoxide dismutase gene from the obligate anaerobic bacterium *Desulfovibrio vulgaris* (Miyazaki F). *J. Biochem.* **133**, 387–393 (2003).
50. Lumpio, H. L., Shenvi, N. V., Summers, A. O., Voordouw, G. & Kurtz, D. M. Rubrerythrin and rubredoxin oxidoreductase in *Desulfovibrio vulgaris*: a novel oxidative stress protection system. *J. Bacteriol.* **183**, 101–108 (2001).
51. Ward, D. E. *et al.* The NADH oxidase from *Pyrococcus furiosus*. *Eur. J. Biochem.* **268**, 5816–5823 (2001).
52. Lin, W. C., Coppi, M. V. & Lovley, D. R. *Geobacter sulfurreducens* can grow with oxygen as a terminal electron acceptor. *Appl. Environ. Microbiol.* **70**, 2525–2528 (2004).
53. Abdollahi, H. & Wimpenny, J. W. T. Effects of oxygen on the growth of *Desulfovibrio desulfuricans*. *Microbiology* **136**, 1025–1030 (1990).
54. Boga, H. I., Brune, A. Hydrogen-dependent oxygen reduction by homoacetogenic bacteria isolated from termite guts. *Appl. Environ. Microbiol.* **69**, 779–786 (2003).
55. Poehlein, A., Gottschalk, G. & Daniel, R. First insights into the genome of the gram-negative, endospore-forming organism *Sporomusa ovata* strain H1 DSM 2662. *Genome. Announc.* **1**, e00734–00713 (2013).



56. Last, G. V. & Schmick, M. T. A review of major non-power-related carbon dioxide stream compositions. *Environ. Earth Sci.* **74**, 1189–1198 (2015).
57. Agreda, V. H. *Acetic Acid and Its Derivatives Chemical Industries*. (CRS Press, New York, 1992).
58. Bond, D. R. & Lovley, D. R. Electricity production by *Geobacter sulfurreducens* attached to electrodes. *Appl. Environ. Microbiol.* **69**, 1548–1555 (2003).
59. Logan, B. E., Rossi, R., Ragab, A. a. & Saikaly, P. E. Electroactive microorganisms in bioelectrochemical systems. *Nat. Rev. Microbiol.* **17**, 307–319 (2019).
60. Clomburg, J. M., Crumbley, A. M. & Gonzalez, R. Industrial biomanufacturing: The future of chemical production. *Science* **355**, 38 (2017).
61. Nishiyama, H. *et al.* Photocatalytic solar hydrogen production from water on a 100 m<sup>2</sup>-scale. *Nature* **598**, 304–307 (2021).
62. Bradford, M. M. A rapid and sensitive method for the quantitation of microgram quantities of protein utilizing the principle of protein-dye binding. *Anal. Biochem.* **72**, 248–254 (1976).